Power Oscillation Damping at Multi-Feeder Nodes Following Equipment Failure Using a STATCOM

Anedi Oko Ganongo[1,*], Mathurin Gogom[1], Haroun Abba Labane[2], Gilbert Ganga[1]

[1]Polytechnic Superior National School, Marien Ngouabi University, Brazzaville, Republic of the Congo

[2]Polytechnic University of Mongo, Mongo, Republic of Chad

Received 13 March 2026; revised 30 May 2026; accepted 22 June 2026

DOI: https://doi.org/10.46604/peti.2026.16262

Abstract

This study aims to investigate the effectiveness of a static synchronous compensator (STATCOM) in damping power oscillations caused by equipment failure at multi-feeder nodes. A theoretical framework based on differential equations and numerical simulation is developed to model transient behavior following feeder loss. The framework is evaluated using the Liouesso-Ouesso network in the Republic of the Congo as a case study by comparing system responses with and without STATCOM compensation. Simulation results show that equipment failures produce oscillations lasting about three cycles, which can trigger cascading protection trips. Integrating a STATCOM reduces oscillation duration to half a cycle and lowers the peak overvoltage from 1.63 pu to 1.0 pu. In multi-feeder configurations, the loss of one feeder causes unequal current redistribution, which can lead to nuisance relay tripping. The STATCOM mitigates these effects by reducing overcurrent duration below typical relay pickup times.

Keywords: damping, equipment failure**,** power oscillations, STATCOM, transient overvoltages

1. Introduction

Electrical networks are systems designed to generate, transmit, and distribute electricity while maintaining power quality and continuous service. Despite careful design, construction, and operation, these networks remain vulnerable to disturbances that could compromise their integrity and normal operation [1-5].

When an electrical network experiences a disturbance, transient regimes form; the nature and severity of these transients determine the potential consequences, which can range from equipment damage to complete blackouts [4-7]. One major cause of these transients is equipment failure. In fact, the unexpected outage of equipment such as a generation unit, transformer, or power line produces transient phenomena characterized by oscillations in electrical quantities, especially voltage, which can reach high amplitudes [6-8].

Power oscillations in electrical networks are closely linked to the voltage behavior at a specific node and the currents flowing through connected lines. Therefore, analyzing the voltage evolution at a critical node can provide insight into active and reactive power oscillations between nodes in the system following a disturbance.

Given the growing demands for speed and sensitivity in modern protection and control systems, such disturbances can trigger cascading trips of other feeders, potentially leading to serious socio-economic consequences. It is therefore crucial to implement techniques or devices that quickly dampen power oscillations.

* Corresponding author. E-mail address: okoanedi@gmail.com

Conventional approaches to power system protection and stabilization, which rely on passive compensation devices such as reactors and capacitor banks, may be slow or inadequate in the face of severe disturbances. In contrast, flexible AC transmission systems (FACTS) devices offer fast response times and greater control flexibility, making them an effective solution for damping power oscillations [3, 9-11].

Previous studies on this topic fall into two main categories. The first includes works that analyze and characterize transient regimes, such as Probst et al. [12] on switching transient overvoltages, Pannila and Edirisinghe [13] on transient signatures in low-voltage systems, Bittar et al. [14] on frequency analysis during switching operations, Awadallah et al. [15] on overvoltage transfer in 400 kV networks, and Zhang et al. [16] on transient overvoltage waveform analysis. These studies have advanced understanding of transient phenomena in electrical networks.

The second category comprises works focused on damping power oscillations using static synchronous compensator (STATCOM)-based damping strategies. Devarapalli and Bhattacharyya [17] applied multi-verse optimization; Bhukya and Mahajan [18] studied controller parameter optimization for systems with wind farms; Zhang et al. [19] developed data-driven methods for wind farm applications; Peres and da Costa [20] compared damping strategies with multi-band controllers; Bamba and Kumar [21] explored intelligent control strategies; and Kouider and Bekri [22] examined PSS and STATCOM cooperation in wind-penetrated systems. More recently, Jiang et al. [23] investigated low-frequency oscillation mechanisms in grid-forming STATCOMs, revealing that DC-link voltage synchronization can introduce phase lags that lead to oscillations, and proposed a lead-lag compensator to effectively damp these oscillations while providing inertial support to the grid. These studies highlight the key role of the STATCOM in enhancing voltage stability and damping electromechanical oscillations.

Despite significant progress in power oscillation damping and overvoltage mitigation, equipment failures at multi-feeder nodes remain insufficiently investigated, particularly at nodes with multiple outgoing feeders, which have substantial technical and economic impacts. To address this gap, the present study proposes a theoretical framework based on electrical and mathematical modeling and numerical simulations.

Unlike previous studies that focus on oscillation damping in radial or single-feeder systems, the present work specifically addresses the protection coordination vulnerability inherent to multi-feeder nodes, where unequal current redistribution following a feeder loss can trigger cascading relay trips.

This work aims to enhance the resilience of electrical networks during equipment failures by: (1) examining power-flow oscillations caused by equipment failures at multi-feeder nodes, and (2) expanding the analysis of STATCOM impact to include damping of power oscillations.

2. Theoretical Approaches

This section outlines the theoretical foundations and mathematical models used to analyze the transient response of an electrical network following a feeder loss, with and without STATCOM compensation. The models are then applied to a real-world network case study.

2.1 Modeling the electrical network during transient conditions

The transient regime caused by a feeder outage in an electrical network is examined using the network's electrical model shown in Fig. 1. This figure presents a simplified single-line diagram of the studied transmission system, consisting of a source, a transmission line, and multiple outgoing feeders.

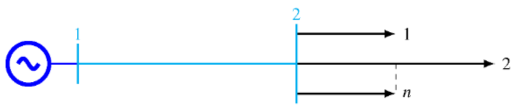

Fig. 1 Electrical network supplying multiple feeders

Following the outage of feeder 2, the corresponding equivalent model of the electrical power transmission network is shown in Fig. 2. This figure illustrates the equivalent circuit after the disconnection of feeder 2 due to upstream equipment failure. The load on feeder 2 has been removed, which modifies the power balance at the common node. This model serves as the basis for deriving the differential equation that describes the voltage dynamics after the loss of feeder 2.

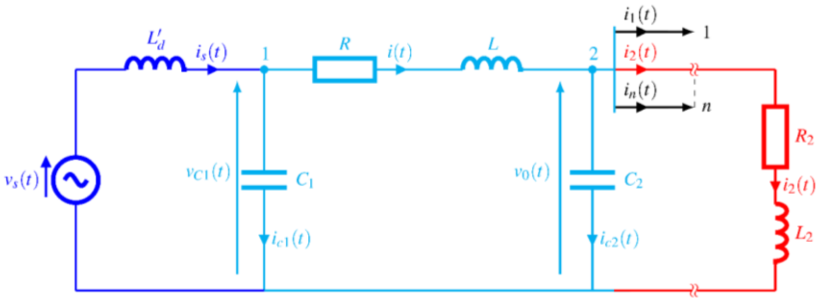

Fig. 2 Circuit model illustrating the loss of feeder 2

In the proposed model, the feeder outage is treated as resulting from an unexpected failure of upstream equipment, such as a power transformer, circuit breaker, or associated switching device. This sudden disconnection initiates a transient response in the remaining network.

The electrical quantities in Fig. 2 are defined as follows: $v_s(t) = V_s \sin(\omega t + \phi)$ is the source voltage; $V_{C1}(t)$ is the voltage across C_1, and L'_d is the generator transient reactance. The transmission line has resistance R and inductance L, while its shunt capacitances are C_1 and C_2, with $C_1 = C_2 = C_l/2$, where C_l denotes the total line capacitance. The current through the line is $i(t)$, and $v_0(t)$ is the voltage at the common node. The feeder currents are $i_1(t)...i_n(t)$, and the load on feeder 2 is represented by R_2 and L_2. The variable t denotes time.

Kirchhoff's and Ohm's laws are applied to the circuit shown in Fig. 2. After eliminating the intermediate variables, the following fifth-order linear differential equation is obtained. This equation describes the dynamic evolution of the voltage following a feeder outage:

$$a_5 \frac{d^5 v_0(t)}{dt^5} + a_4 \frac{d^4 v_0(t)}{dt^4} + a_3 \frac{d^3 v_0(t)}{dt^3} + a_2 \frac{d^2 v_0(t)}{dt^2} + a_1 \frac{dv_0(t)}{dt} + a_0 v_0(t) = L_{eq} \frac{dv_s(t)}{dt} + R_{eq} v_s(t) \tag{1}$$

where the coefficients are defined as follows:

$$\begin{cases} a_5 = L'_d C_1 L C_2 L_{eq} \\ a_4 = L'_d C_1 C_2 (R L_{eq} + L R_{eq}) \\ a_3 = L'_d C_1 (R C_2 R_{eq} + L + L_{eq}) + C_2 L_{eq} (L'_d + L) \\ a_2 = R(L'_d C_1 + C_2 L_{eq}) + R_{eq}[L'_d (C_1 + C_2) + L C_2] \\ a_1 = L'_d + R C_2 R_{eq} + L + L_{eq} \\ a_0 = R + R_{eq} \end{cases} \tag{2}$$

where R_{eq} and L_{eq} represent the equivalent resistance and inductance of the remaining feeders, respectively, corresponding to the feeders' total active and reactive powers.

The time-domain behavior of the voltage at the fault point is obtained by solving Eq. (1). Several numerical methods (e.g., Euler and Runge-Kutta) are available for this purpose. The fourth-order Runge-Kutta method (RK4) is selected for this study because it offers a good balance between accuracy and numerical stability. The RK4 solution follows the procedure described below:

(1) Transformation into a set of first-order equations

The fifth-order differential equation is converted into a system of five first-order differential equations by introducing the following state variables:

$$\mathbf{y} = \begin{bmatrix} y_1 \\ y_2 \\ y_3 \\ y_4 \\ y_5 \end{bmatrix} = \begin{bmatrix} v_0 \\ \frac{dv_0}{dt} \\ \frac{d^2v_0}{dt^2} \\ \frac{d^3v_0}{dt^3} \\ \frac{d^4v_0}{dt^4} \end{bmatrix} \tag{3}$$

The system of equations is then written as:

$$\frac{d\mathbf{y}}{dt} = \mathbf{f}(t, \mathbf{y}) = \begin{bmatrix} y_2 \\ y_3 \\ y_4 \\ y_5 \\ \frac{1}{a_5}\left[L_{eq}\frac{dv_s(t)}{dt} + R_{eq}v_s(t) - a_4y_5 - a_3y_4 - a_2y_3 - a_1y_2 - a_0y_1\right] \end{bmatrix} \tag{4}$$

(2) Definition of initial conditions

The initial conditions are defined by the initial state vector:

$$\mathbf{y}_0 = \begin{bmatrix} v_0(0) \\ \frac{dv_0}{dt}(0) \\ \frac{d^2v_0}{dt^2}(0) \\ \frac{d^3v_0}{dt^3}(0) \\ \frac{d^4v_0}{dt^4}(0) \end{bmatrix} \tag{5}$$

(3) Calculation of increments

For each time step h, four increments k_1, k_2, k_3, and k_4 are calculated, representing estimates of the solution slope at different points in the interval [t_n, t_{n+1}]:

$$\begin{cases} \mathbf{k}_1 = h \cdot \mathbf{f}(t_n, \mathbf{y}_n) \\ \mathbf{k}_2 = h \cdot \mathbf{f}\left(t_n + \frac{h}{2}, \mathbf{y}_n + \frac{\mathbf{k}_1}{2}\right) \\ \mathbf{k}_3 = h \cdot \mathbf{f}\left(t_n + \frac{h}{2}, \mathbf{y}_n + \frac{\mathbf{k}_2}{2}\right) \\ \mathbf{k}_4 = h \cdot \mathbf{f}(t_n + h, \mathbf{y}_n + \mathbf{k}_3) \end{cases} \tag{6}$$

where k_1 is the slope at the beginning of the interval, k_2 and k_3 are intermediate estimates at the midpoint, and k_4 is the slope at the end of the interval.

(4) Update on the solution

The four increments are combined to produce an accurate estimate of the solution at time t_{n+1} according to the formula:

$$\mathbf{y}_{n+1} = \mathbf{y}_n + \frac{1}{6}(\mathbf{k}_1 + 2\mathbf{k}_2 + 2\mathbf{k}_3 + \mathbf{k}_4) \tag{7}$$

where y_n is the state vector at time t_n.

This procedure is repeated iteratively over the time interval [*0*, *T*] to obtain the complete evolution of the voltage $v_0(t)$. The fourth-order Runge-Kutta method has a local truncation error on the order of $O(h^5)$ and a global error on the order of $O(h^4)$. These properties guarantee high-order convergence of the numerical solution towards the exact solution as the step size *h* approaches zero, thereby ensuring sufficient accuracy for the analysis of electromagnetic transient regimes of the network.

The numerical solution provides a complete description of the network's dynamic response following a line loss. It shows how the voltage at the critical node evolves, highlighting the amplitude and duration of the resulting overvoltages. These results are essential for evaluating the severity of the transient regime and for identifying potential risks such as insulation failure or unwanted relay tripping. However, this model does not include any compensation device. The following section extends this model by introducing a STATCOM to dampen the resulting oscillations.

2.2 STATCOM modeling

The overall architecture of a STATCOM is shown in Fig. 3. It consists of four main functional blocks:

(1) AC network: The point of common coupling (PCC) at which the STATCOM connects to the power grid. The voltage and current at this node are continuously monitored.

(2) Voltage source converter (VSC): The power electronic stage, typically based on IGBTs, that converts the DC bus voltage into a controllable AC voltage. The amplitude and phase of this voltage determine the reactive power exchanged with the grid.

(3) Control system: The core of the STATCOM. It processes measured voltages and currents using vector control in the synchronously rotating *dq* reference frame. The control system generates the reference AC voltages needed to regulate the PCC voltage or the reactive power.

(4) PWM modulation: The pulse-width modulator converts the control system's reference voltages into gate signals for the VSC's IGBTs. This ensures that the converter produces the desired AC voltage waveform.

The close interaction between the control system and the VSC enables the STATCOM to inject or absorb reactive power almost instantaneously, making it particularly effective at damping power oscillations during transient events such as feeder loss.

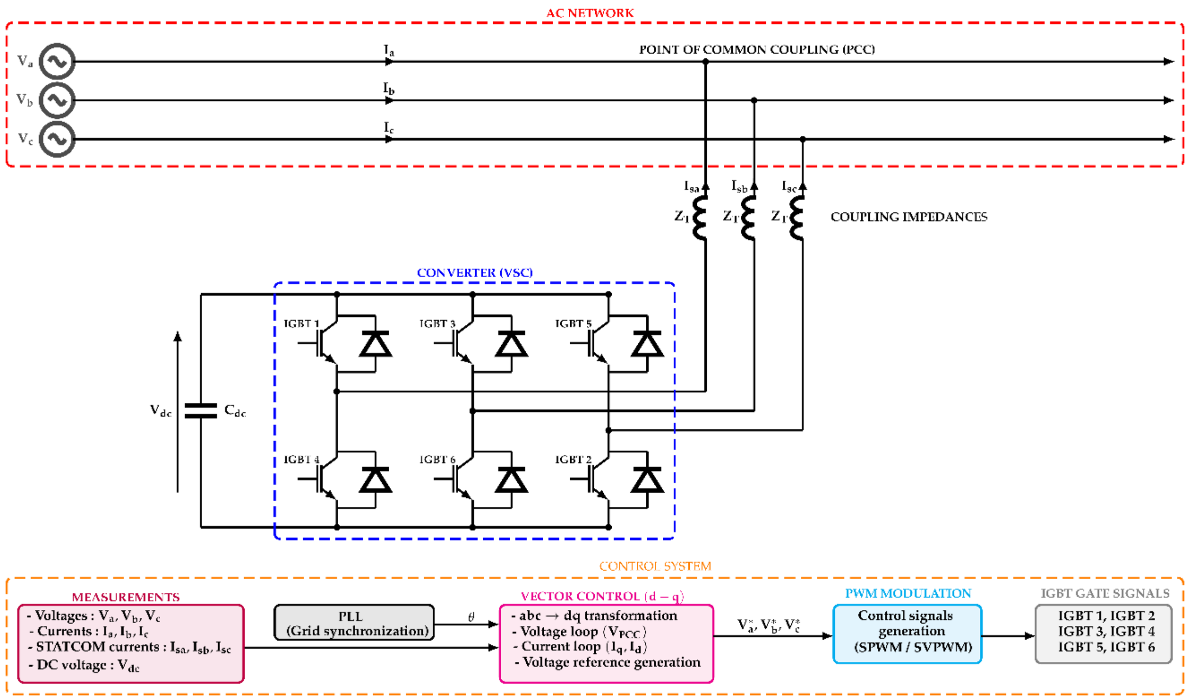

Fig. 3 Complete architecture of a STATCOM

(1) STATCOM control system

The principle of STATCOM voltage regulation is illustrated in Fig. 4 [24]. This figure presents the cascade control architecture, comprising an outer voltage regulation loop and an inner current control loop. The outer loop generates a reference quadrature current based on the voltage error, while the inner loop processes the current errors and outputs the reference voltage for the PWM modulator. This dual-loop structure ensures fast and accurate voltage regulation, enabling the STATCOM to inject or absorb reactive power in response to network disturbances.

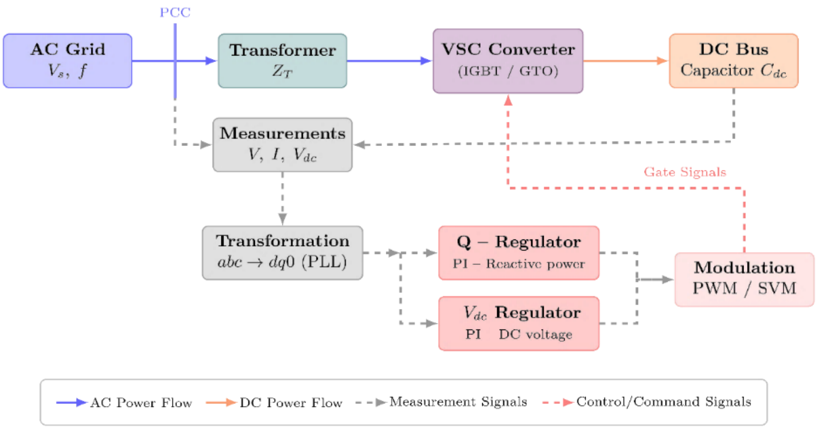

Fig. 4 Block diagram of the STATCOM control system

The control architecture comprises an outer voltage regulation loop and an inner current control loop [24].

(i) Outer voltage loop

The voltage at the PCC, V_{PCC}, is measured and compared with a reference voltage V_{ref}. The error signal $\varepsilon = V_{ref} - V_{PCC}$ is processed by a proportional-integral (PI) controller. The output of this controller is the reference quadrature current $I_{q,ref}$, which determines the reactive power exchange:

$$I_{q,ref} = K_{p,v} \cdot \varepsilon + K_{i,v} \int \varepsilon dt \tag{8}$$

The transfer function of the voltage regulator is:

$$G_v(s) = K_{p,v} + \frac{K_{i,v}}{s} \tag{9}$$

where $K_{p,v}$ and $K_{i,v}$ are the proportional and integral gains of the voltage regulator, respectively.

(ii) Inner current loop

The three-phase currents I_a, I_b, I_c are transformed into the synchronous dq reference frame using a phase-locked loop (PLL). The direct current reference $I_{d,ref}$ is set to zero to maintain unity power factor (ideal STATCOM assumption). The quadrature current reference $I_{q,ref}$ is provided by the outer loop. A second PI controller processes the current errors:

$$G_i(s) = K_{p,i} + \frac{K_{i,i}}{s} \tag{10}$$

where $K_{p,i}$ and $K_{i,i}$ are the proportional and integral gains of the current regulator, respectively.

The output of the current controller is a reference voltage $V_{STATCOM,ref}$ in the dq frame, which is transformed back into three-phase voltages to generate PWM commands for the VSC.

(iii) Closed-loop transfer function

Combining the outer and inner loops with the equivalent capacitance seen from the PCC C and the PWM delay T_{PWM}, the overall closed-loop voltage regulation transfer function is:

$$H(s)=\frac{G_v(s)\cdot G_i(s)\cdot\dfrac{1}{1+sT_{\text{PWM}}}\cdot\dfrac{1}{sC}}{1+G_v(s)\cdot G_i(s)\cdot\dfrac{1}{1+sT_{\text{PWM}}}\cdot\dfrac{1}{sC}} \tag{11}$$

(iv) Operating modes

The STATCOM can operate in two modes, as summarized in Table 1. In this study, the voltage regulation mode is used. This mode maintains the PCC voltage at a reference value by adjusting the reactive power output. The second mode, reactive power control, maintains a constant reactive power output regardless of voltage variations.

Table 1 STATCOM operating modes

Mode	Controlled quantity	Regulator input	Regulator output	Application
Voltage regulation	V_{PCC}	V_{ref}-V_{PCC}	$I_{q,ref}$	Oscillation damping, voltage support
Reactive power control	Q	Q_{ref} - Q_{mes}	$I_{q,ref}$	Steady-state power factor correction

In this work, the STATCOM operates in voltage regulation mode because the primary objective is to damp power oscillations by maintaining the PCC voltage at its nominal level. This mode enables rapid reactive power adjustment in response to voltage variations. This choice is particularly suitable for equipment failure scenarios, where voltage stability is essential to avoid cascading trips and ensure network continuity.

(2) Simplified steady-state model

STATCOM modeling relies on a set of simplifying assumptions that allow its operation to be represented in an idealized manner. These assumptions simplify the mathematical analysis of the device while maintaining sufficient accuracy for practical use and power system stability studies. The simplifying assumptions for STATCOM modeling under ideal operating conditions are as follows:

(i) The converter switches are assumed to be ideal, with no losses or switching delays.
(ii) The three-phase voltages produced by the STATCOM are assumed to be balanced, with equal amplitude and a 120° phase shift.
(iii) The harmonic components resulting from switching are ignored, and the analysis is limited to the fundamental component.
(iv) The voltage produced by the STATCOM is assumed to be synchronized with the network voltage.

Given these assumptions, the STATCOM operation is analyzed in quasi-steady state to characterize its power exchanges with the network. In contrast, the overall study of the electrical network, presented in the rest of this work, is conducted in the time domain to examine transient regimes following line losses.

Considering the established simplifying assumptions, the STATCOM is represented by the simplified equivalent diagram in Fig. 5, commonly used to analyze its interactions with the electrical network [25-27]. This representation illustrates the key mechanism by which the STATCOM affects the voltage at the connection node through reactive power control.

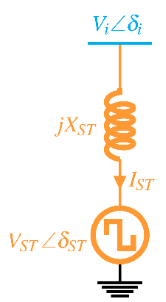

Fig. 5 Simplified STATCOM model

The current absorbed by the STATCOM is denoted as I_{ST}, where V_i is the voltage amplitude at node i and δ_i is its phase, V_{ST} is the STATCOM voltage amplitude, δ_{ST} is its phase, and X_{ST} is the equivalent reactance of the STATCOM.

Depending on the analysis domain considered, the STATCOM current can be described either in the time domain to capture the electromagnetic dynamics associated with the coupling inductance or in quasi-steady state using complex quantities to characterize the power exchanges with the network.

The current absorbed by the STATCOM can be expressed, depending on the chosen representation domain, as follows:

$$\begin{cases} \dfrac{di_{ST}(t)}{dt} = \dfrac{1}{L_{ST}}\left[v_i(t) - v_{ST}(t)\right] \\ \bar{I}_{ST} = \dfrac{\bar{V}_i - \bar{V}_{ST}}{jX_{ST}} \end{cases} \tag{12}$$

The conjugate expression of the power absorbed by the STATCOM is defined by:

$$S_{ST}^* = \left(\bar{V}_{ST} I_{ST}^*\right)^* = P_{ST} - jQ_{ST} \tag{13}$$

Substituting the second expression of system Eq. (12) into Eq. (13) yields the following equation:

$$S_{ST}^* = V_{ST}^* \bar{I}_{ST} = V_{ST}^* \frac{\bar{V}_i - \bar{V}_{ST}}{jX_{ST}} \tag{14}$$

Developing Eq. (14) yields:

$$S_{ST}^* = \frac{V_i V_{ST}}{X_{ST}} \sin(\delta_i - \delta_{ST}) - j\frac{V_{ST}}{X_{ST}}\left[V_i \cos(\delta_i - \delta_{ST}) - V_{ST}\right] \tag{15}$$

The following formulas can then express the active and reactive powers drawn by the STATCOM:

$$\begin{cases} P_{ST} = \dfrac{V_i V_{ST}}{X_{ST}} \sin(\delta_i - \delta_{ST}) \\ Q_{ST} = \dfrac{V_{ST}}{X_{ST}}\left[V_i \cos(\delta_i - \delta_{ST}) - V_{ST}\right] \end{cases} \tag{16}$$

In the case of an ideal STATCOM, no active power is exchanged with the network. This constraint requires phase alignment between the voltage generated by the STATCOM and that of the connection node, which is expressed by the following relation:

$$\delta_{ST} - \delta_i = 0 \Rightarrow \delta_{ST} = \delta_i \tag{17}$$

The STATCOM voltage is therefore in phase with the network voltage. However, in practice, a small amount of active power is absorbed to compensate for losses in the STATCOM converter and in the coupling transformer.

The reactive power exchanged with the network is then determined by:

$$Q_{ST} = \frac{V_i V_{ST}}{X_{ST}}\left(1 - \frac{V_{ST}}{V_i}\right) \tag{18}$$

From Eq. (18), the following conclusions can be drawn:

(i) If the magnitude of the STATCOM voltage is equal to that of the network voltage, $Q_{ST} = 0$, no energy transfer occurs;

(ii) If $V_{ST} > V_i$, then $Q_{ST} > 0$, the STATCOM operates as a capacitor and supplies reactive power to the network;

(iii) If $V_{ST} < V_i$, then $Q_{ST} < 0$, the STATCOM functions as an inductor and absorbs reactive power from the network.

These relations demonstrate that the STATCOM functions as a controllable reactive power source, capable of locally adjusting the voltage level at the connection node. By dynamically modifying the amplitude of its internal voltage V_{ST}, the STATCOM enables control of reactive power flows in the network.

During a severe disturbance, such as the sudden loss of a line, this ability to rapidly regulate reactive power becomes a crucial tool for damping electromagnetic and electromechanical oscillations. The STATCOM can then serve as an effective control device to enhance transient stability and limit voltage fluctuations at the critical node.

The STATCOM model described above can now be integrated into the electrical network to analyze its impact on the transient regime.

2.3 Modeling of the electrical network with STATCOM during the transient regime

Fig. 6 shows the electrical model of the studied network with the STATCOM integrated after the loss of feeder 2. This figure extends the previous model by incorporating a STATCOM connected at the point of common coupling (PCC). The STATCOM is represented by its coupling inductance L_{ST} and its generated voltage $v_{ST}(t)$, which can be controlled to inject or absorb reactive power.

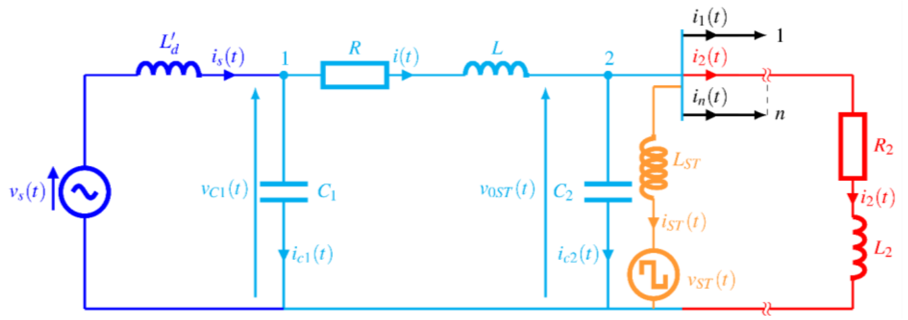

Fig. 6 Equivalent model of the electrical network with STATCOM compensation after a feeder failure

In the circuit, the voltage at the connection node between the feeders and the STATCOM is denoted as $v_{0ST}(t)$. The current absorbed by the STATCOM is $i_{ST}(t)$, and L_{ST} represents its coupling inductance. The fundamental voltage produced by the STATCOM is expressed as $v_{ST}(t) = V_{ST}\sin(\omega t + \phi_{ST})$, where V_{ST} and ϕ_{ST} correspond to the amplitude and phase of this voltage, respectively.

Applying Kirchhoff's laws to the circuit in Fig. 6 and eliminating intermediate variables results in the following sixth-order linear differential equation for $v_{0ST}(t)$:

$$b_6\frac{d^6v_{0ST}(t)}{dt^6}+b_5\frac{d^5v_{0ST}(t)}{dt^5}+b_4\frac{d^4v_{0ST}(t)}{dt^4}+b_3\frac{d^3v_{0ST}(t)}{dt^3}+b_2\frac{d^2v_{0ST}(t)}{dt^2}+b_1\frac{dv_{0ST}(t)}{dt}+b_0v_{0ST}(t)=F(t) \tag{19}$$

where the coefficients are given by:

$$\begin{cases} b_6 = L'_dC_1LC_2L_{ST}L_{eq} \\ b_5 = L'_dC_1C_2L_{ST}(RL_{eq}+LR_{eq}) \\ b_4 = L'_dC_1(RC_2L_{ST}R_{eq}+LL_{ST}+LL_{eq}+L_{ST}L_{eq})+C_2L_{ST}L_{eq}(L'_d+L) \\ b_3 = R[L'_dC_1L_{eq}+L_{ST}(L'_dC_1+C_2L_{eq})]+R_{eq}(L_{ST}[L'_dC_1L+L'_d(C_1+C_2)+LC_2]) \\ b_2 = L'_dC_1RR_{eq}+L_{eq}(L'_d+L)+L_{ST}(L'_d+RC_2R_{eq}+L+L_{eq}) \\ b_1 = RL_{eq}+L_{ST}(R+R_{eq})+R_{eq}(L'_d+L) \\ b_0 = RR_{eq} \end{cases} \tag{20}$$

and the right side:

$$\begin{aligned} F(t) = {} & L'_dC_1LL_{eq}\frac{d^4v_{ST}(t)}{dt^4}+L'_dC_1(RL_{eq}+LR_{eq})\frac{d^3v_{ST}(t)}{dt^3}+[L'_dC_1RR_{eq}+L_{eq}(L'_d+L)]\frac{d^2v_{ST}(t)}{dt^2} \\ & +[RL_{eq}+R_{eq}(L'_d+L)]\frac{dv_{ST}(t)}{dt}+RR_{eq}v_{ST}(t)+L_{ST}L_{eq}\frac{d^2v_s(t)}{dt^2}+L_{ST}R_{eq}\frac{dv_s(t)}{dt} \end{aligned} \tag{21}$$

The solution to the sixth-order differential equation (Eq. (19)) is obtained using the fourth-order Runge-Kutta (RK4) numerical method, as previously outlined.

2.4 Application to the Liouesso-Ouesso power network

In this section, these models are applied to a practical case study: the Liouesso-Ouesso network in the Sangha Department (Republic of the Congo), shown in Fig. 7. This figure presents the single-line diagram of the actual network, which consists of two transformers and three outgoing feeders. This configuration serves as the reference case for evaluating the impact of a feeder loss and STATCOM performance.

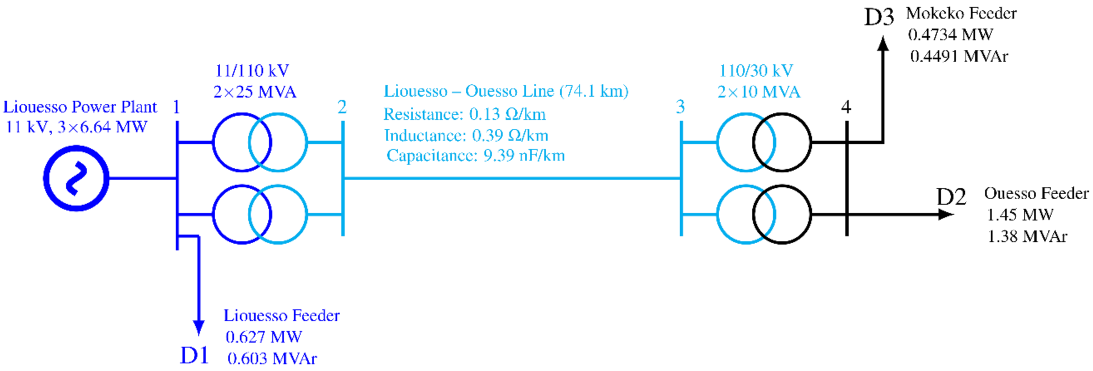

Fig. 7 Initial configuration of the transmission network with feeders D1, D2, and D3

Fig. 7 shows the actual initial network with its three feeders, D1, D2, and D3. After D2 fails due to the malfunction of the equipment supplying or connecting it, such as a circuit breaker, transformer, or associated switching device, the equivalent model in Fig. 8 is obtained by applying Thevenin's theorem at busbar JB1 and combining the impedances between JB1 and JB4.

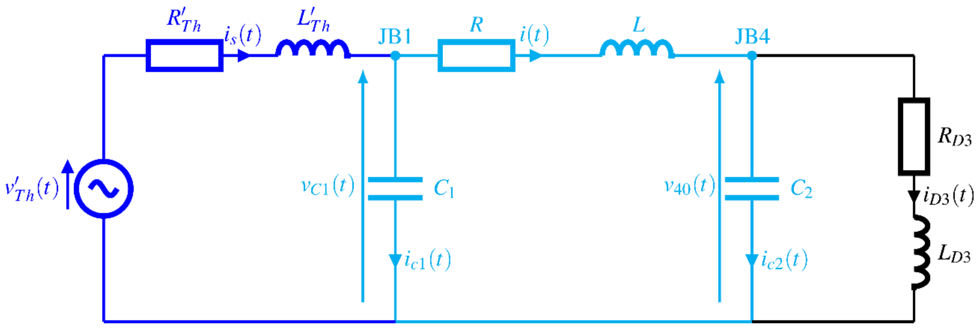

Fig. 8 Equivalent diagram of the network after the outage of feeder D2

All network parameters have been referred to the 30 kV level, which is the nominal voltage at the multi-feeder node (node 4) where the STATCOM is connected. The complete set of parameters (resistances, inductances, capacitances, transformer data, etc.) referred to 30 kV is listed in Appendix A.1. Furthermore, to avoid any confusion and to make the results independent of the voltage level, all quantities are expressed in per-unit (pu). The base values are $V_{base}=30kV$ (secondary side of the transformer T2) and $S_{base}=100MVA$.

The characteristic parameters of this model include the equivalent Thevenin voltage $v'_{Th}(t)$, the Thevenin resistance R'_{Th} and inductance L'_{Th} of the upstream part, the total line resistance R and inductance L (including transformer contributions), the line shunt capacitances C_1 and C_2 (with $C_1 = C_2 = C_l/2$, where C_l is the total line capacitance), and the referred parameters of feeder D3, namely R_{D3} and L_{D3}.

The voltage dynamics at node 4 following the loss of feeder D2 are described by the following differential equation, consistent with the model established in Eq. (1):

$$c_5\frac{d^5v_{40}(t)}{dt^5}+c_4\frac{d^4v_{40}(t)}{dt^4}+c_3\frac{d^3v_{40}(t)}{dt^3}+c_2\frac{d^2v_{40}(t)}{dt^2}+c_1\frac{dv_{40}(t)}{dt}+c_0v_{40}(t)=L_{D3}\frac{v'_{Th}(t)}{dt}+R_{D3}v'_{Th}(t) \tag{22}$$

where the coefficients are given by:

$$\begin{cases} c_5 = L'_{Th}C_1LC_2L_{D3} \\ c_4 = C_1C_2[R'_{Th}LL_{D3} + L'_{Th}(RL_{D3} + LR_{D3})] \\ c_3 = L'_{Th}C_1L + C_1C_2[R'_{Th}RL_{D3} + R_{D3}(R'_{Th}L + L'_{Th}R)] + L_{D3}[L'_{Th}(C_1 + C_2) + LC_2] \\ c_2 = (R'_{Th}L_{D3} + L'_{Th}R_{D3})(C_1 + C_2) + C_1(R'_{Th}L + L'_{Th}R) + C_2[RL_{D3} + R_{D3}(R'_{Th}C_1R + L)] \\ c_1 = R'_{Th}C_1(R + R_{D3}) + L'_{Th} + L + C_2R_{D3}(R'_{Th} + R) + L_{D3} \\ c_0 = R'_{Th} + R + R_{D3} \end{cases} \tag{23}$$

To mitigate the effects of this loss, a STATCOM device is installed at the critical node (node 4). Derived from the model established in Eq. (19), the voltage equation incorporating the STATCOM's action at this node is as follows:

$$d_6\frac{d^6v_{4ST}}{dt^6} + d_5\frac{d^5v_{4ST}}{dt^5} + d_4\frac{d^4v_{4ST}}{dt^4} + d_3\frac{d^3v_{4ST}}{dt^3} + d_2\frac{d^2v_{4ST}}{dt^2} + d_1\frac{dv_{4ST}}{dt} + d_0v_{4ST} = G(t) \tag{24}$$

where the modified coefficients are defined as:

$$\begin{cases} d_6 = & L'_{Th}C_1LC_2L_{ST}L_{D3} \\ d_5 = & C_1C_2L_{ST}[R'_{Th}LL_{D3} + L'_{Th}(LR_{D3} + RL_{D3})] \\ d_4 = & L'_{Th}C_1L(L_{ST} + L_{D3}) + C_1C_2L_{ST}[R'_{Th}RL_{D3} + R_{D3}(R'_{Th}L + L'_{Th}R)] + L_{ST}L_{D3}[L'_{Th}(C_1 + C_2) + LC_2] \\ d_3 = & L_{ST}(R'_{Th}L_{D3} + L'_{Th}R_{D3})(C_1 + C_2) + C_1L_{ST}(R'_{Th}L + L'_{Th}R) + C_1[L'_{Th}LR_{D3} + L_{D3}(R'_{Th}L + L'_{Th}R)] \\ & +C_2L_{ST}[RL_{D3} + R_{D3}(R'_{Th}C_1R + L)] \\ d_2 = & R'_{Th}C_1L_{ST}(R + R_{D3}) + L'_{Th}L_{ST} + LL_{ST} + C_2L_{ST}R_{D3}(R'_{Th} + R) + L_{D3} \\ & +C_1R_{D3}(R'_{Th}L + L'_{Th}R) + L_{D3}(R'_{Th}C_1R + L'_{Th} + L) \\ d_1 = & R_{D3}(R'_{Th}C_1R + L'_{Th} + L) + L_{D3}(R'_{Th} + R) + L_{ST}(R'_{Th} + R + R_{D3}) \\ d_0 = & R_{D3}(R'_{Th} + R) \end{cases} \tag{25}$$

and the right side is defined as:

$$\begin{aligned} G(t) = \;& L'_{Th}C_1LL_{D3}\frac{d^4v_{ST}(t)}{dt^4} + C_1[L'_{Th}LR_{D3} + L_{D3}(R'_{Th}L + L'_{Th}R)]\frac{d^3v_{ST}(t)}{dt^3} \\ & +[C_1R_{D3}(R'_{Th}L + L'_{Th}R) + L_{D3}(R'_{Th}C_1R + L'_{Th} + L)]\frac{d^2v_{ST}(t)}{dt^2} \\ & +[R_{D3}(R'_{Th}C_1R + L'_{Th} + L) + L_{D3}(R'_{Th} + R)]\frac{dv_{ST}(t)}{dt} + R_{D3}(R'_{Th} + R)v_{ST}(t) \\ & +L_{ST}L_{D3}\frac{d^2v'_{Th}(t)}{dt^2} + L_{ST}R_{D3}\frac{dv'_{Th}(t)}{dt} \end{aligned} \tag{26}$$

The instantaneous power transferred between nodes 1 and 4 is given by:

$$P_{14}(t) = v_4(t)\cdot i_{14}(t) \tag{27}$$

The current $i_{14}(t)$ is obtained by solving Eq. (28) using the RK4 method:

$$\begin{cases} L\dfrac{di_{14}(t)}{dt} + Ri_{14}(t) = v'_{Th}(t) - v_4(t) - L'_{Th}\dfrac{di_s(t)}{dt} - R'_{Th}i_s(t) \\ L'_{Th}C_1\dfrac{d^2i_s(t)}{dt^2} + R'_{Th}C_1\dfrac{di_s(t)}{dt} + i_s(t) = C_1\dfrac{dv'_{Th}(t)}{dt} + i_{14}(t) \end{cases} \tag{28}$$

Feeder D3 is an extension of the network supplying several loads through multiple low-voltage (LV) transformers. To analyze the behavior of a typical load supplied by this feeder during the loss of feeder D2, a single induction motor is considered. The motor is supplied through a step-down transformer (30 kV / 0.4 kV). The parameters analyzed include motor torque and speed, expressed by the following relations:

$$\begin{cases} \Omega_r = (1-g)\Omega_s \\ C_e = pM(i_{dr}i_{qs} - i_{qr}i_{ds}) \end{cases} \tag{29}$$

where Ω_r represents the mechanical angular speed of the rotor (in rad/s), C_e is the electromagnetic torque (in N·m), g denotes the slip, Ω_s is the synchronous speed (in rad/s), p is the number of pole pairs, and M is the mutual inductance in H. The stator and rotor currents in the direct and quadrature axes, denoted as i_{ds}, i_{qs}, i_{dr}, and i_{qr} are expressed in A. Finally, the electrical speed of the rotor ω (in rad/s) is related to the mechanical speed by the relation $\omega = p\ \Omega_r$.

3. Simulations, Results, and Discussion

To validate the theoretical models developed in the previous section, numerical simulations were performed using MATLAB. This section presents the simulation results for the voltage at the critical node, the power flow between nodes, and the behavior of a motor connected to the network. The performance of the STATCOM is assessed by comparing the system's response with and without compensation. Finally, the results are analyzed in terms of their implications for network stability and equipment protection.

3.1 Simulations and results obtained

The simulation incorporates four main components: the Liouesso-Ouesso network voltage model without STATCOM (Eq. (22)), the Liouesso-Ouesso network voltage model with STATCOM (Eq. (24)), the transmitted power model (Eq. (27)), and the induction motor (Eq. (29)). These equations are solved sequentially using the RK4 method described in Section 2.1. The outputs are the voltage at node 4 (Fig. 9), the transmitted power (Fig. 10), and the motor speed and torque (Figs. 11 and 12). All simulations were performed with a fixed time step $\Delta t = 0.1$ ms, selected based on a convergence study (time steps of 0.5 ms, 0.2 ms, and 0.05 ms showed no significant variation below 0.1 ms), ensuring numerical stability and accuracy. The measurement points for the three main variables are as follows:

(1) The voltage is measured at node 4, where the STATCOM is connected.

(2) The transmitted power is evaluated at the line between nodes 1 and 4.

(3) The motor speed and electromagnetic torque are measured at the output of the induction machine connected to feeder 3.

The voltage dynamics at node 4 after the outage of feeder 2 were calculated by numerically solving Eqs. (22) and (24) in MATLAB, with the reference voltage $v_4 = 1.0 \cdot \sin(\omega t - 0.05565)$ p.u. The results are presented in Fig. 9, which compares the voltage response at the multi-feeder node with and without STATCOM compensation.

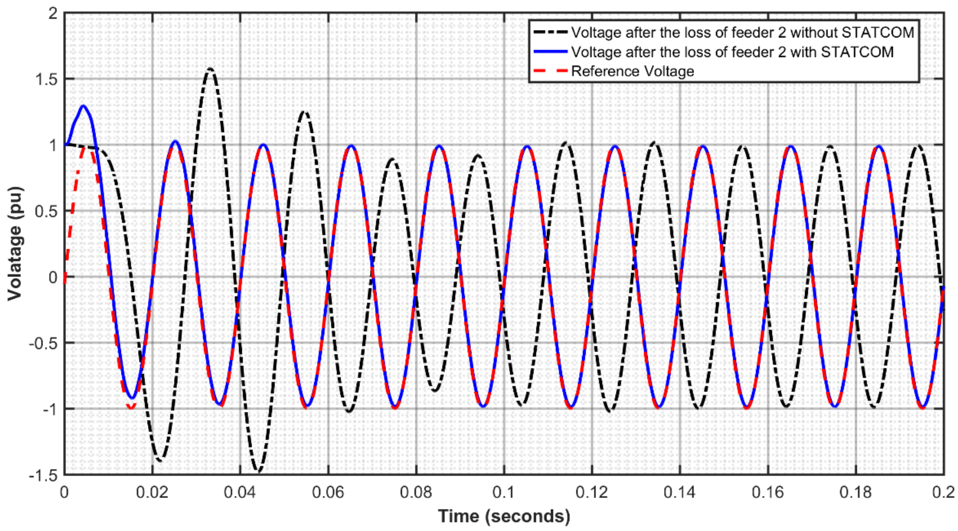

Fig. 9 Voltage response at node 4 following the outage of feeder 2 with and without STATCOM

The instantaneous power flow between nodes 1 and 4 after the loss of feeder 2 was calculated by simulating Eq. (27) in MATLAB. The results are displayed in Fig. 10. This figure shows the evolution of the transmitted power over time, with and without STATCOM compensation.

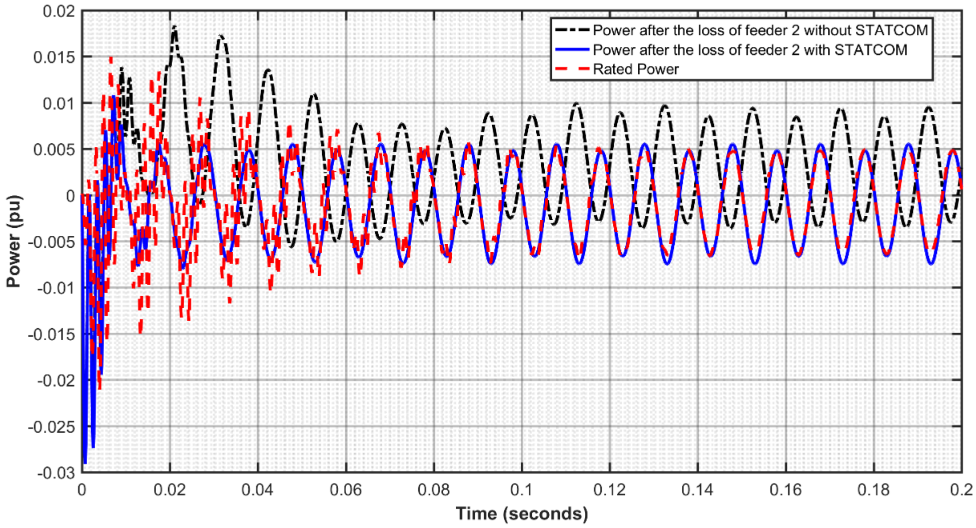

Fig. 10 Instantaneous power transfer between nodes 1 and 4 with and without STATCOM

The operation of a motor connected to feeder 3 was simulated under the specified conditions by solving the system of Eq. (29). The results for speed and torque are shown in Figs. 11 and 12, respectively. These figures illustrate the dynamic response of the induction motor during startup, with and without STATCOM compensation.

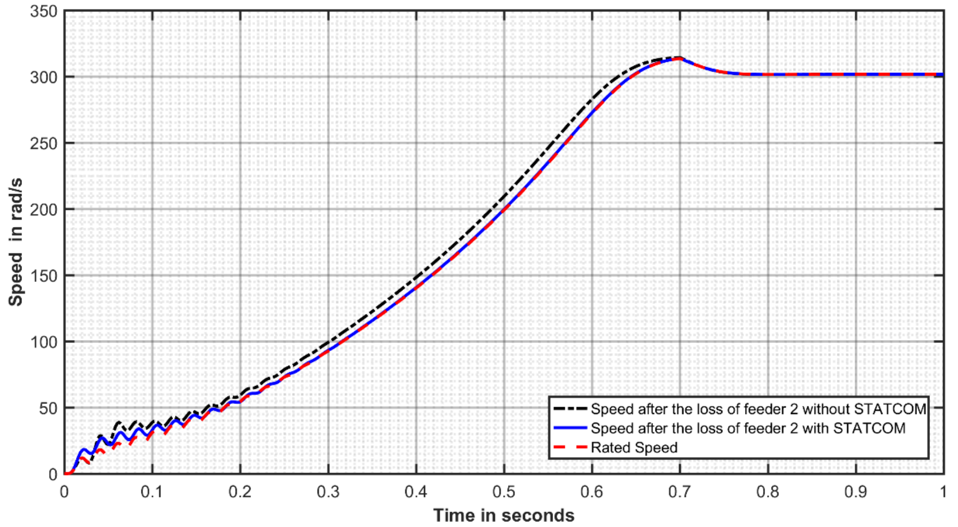

Fig. 11 induction motor speed at feeder 3 with and without STATCOM

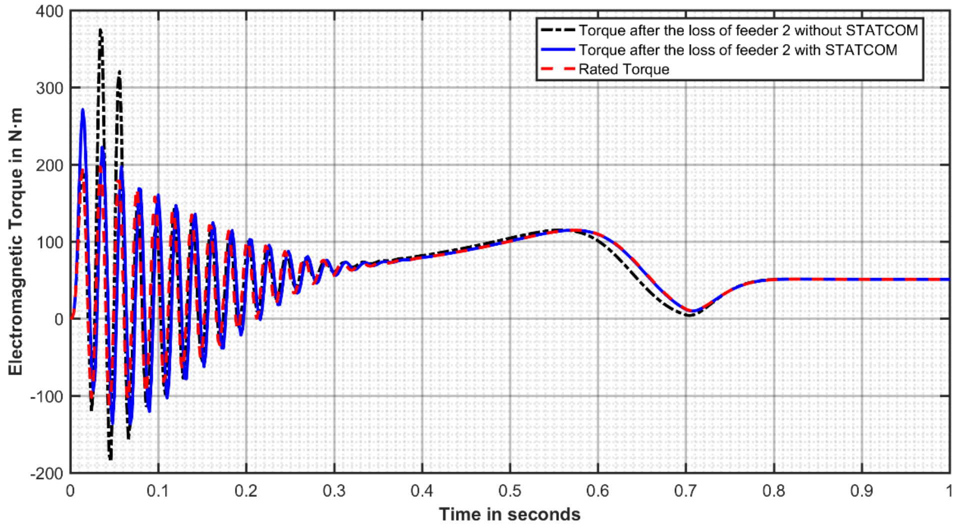

Fig. 12 Evolution of motor torque connected to feeder 3 with and without STATCOM

3.2 Discussion

Having presented the simulation outcomes in Figs. 9-12, this discussion now analyses their physical meaning and practical implications. Particular attention is paid to the overall transient response of the network, the protection coordination issues specific to multi-feeder configurations, and the compliance of the observed overvoltages with international insulation standards.

(1) Transient network response

The loss of feeder 2 significantly alters the network operating conditions, triggering transients that propagate from voltage to power and finally to connected loads. As shown in Fig. 9, the voltage at node 4 rises well above its nominal value, peaking at 1.63 pu and persisting for about three cycles (60 ms at 50 Hz). Such overvoltages may exceed the short-term withstand capabilities of certain fast-acting protection devices. Consequently, if the disturbance lasts longer than one cycle, the consequences can escalate rapidly: equipment damage, insulation failure, unwanted relay tripping, and even cascading outages.

This voltage instability directly affects the power flowing between nodes 1 and 4 (Fig. 10). The transmitted power oscillates concurrently with the voltage disturbance, reaching peaks that may increase the thermal and mechanical integrity of the transmission lines. Thus, voltage and power oscillations are not independent phenomena; rather, they reinforce each other, turning a local disturbance into a system-wide threat.

The impact does not stop at power lines. As illustrated in Figs. 11 and 12, electromagnetic disturbances propagate to active loads, in this case, an induction motor connected to feeder 3. During the startup phase, the motor without STATCOM suffers marked overshoots in both speed and torque. With STATCOM, however, the speed follows the nominal acceleration profile closely, and the torque remains near its rated value. This smoother startup reduces mechanical stress, a critical advantage for sensitive industrial processes that demand stable acceleration, such as conveyors, textile machines, or precision drives.

Fortunately, the STATCOM proves to be an effective mitigation measure. While the uncompensated system struggles with three full cycles of oscillations, the STATCOM restores the voltage to its nominal level in just half a cycle (Fig. 9). This remarkable performance stems from its ability to inject or absorb reactive power within a very short response time. The transmitted power (Fig. 10) quickly returns to steady-state conditions, demonstrating the capability of the sixth-order differential model (Eq. (24)). Moreover, the STATCOM significantly attenuates the disturbance reaching the motor (Figs. 11 and 12), thereby preserving mechanical integrity and ensuring continuity of industrial operations.

The STATCOM reduces the settling time by a factor of six, from three cycles to half a cycle, and eliminates residual oscillations. It not only stabilizes the network but also protects sensitive equipment, making it a promising solution for multi-feeder nodes subject to equipment failures.

(2) Protection coordination issues in multi-feeder configurations

Beyond the transient phenomena described above, multi-feeder configurations introduce an additional risk: protection coordination vulnerability. When feeder 2 is lost, the total load current redistributes among the remaining feeders (D1 and D3). Because their line impedances differ, this redistribution is unequal, creating a current imbalance. The current in feeder D3 increases more significantly than in D1, leading to a larger transient overcurrent on D3 (Table 2). The current in D1 also increases, but to a lesser extent. More critically, the transient overcurrent during the first cycles after the fault may exceed the pickup thresholds of overcurrent relays protecting the healthy feeders.

Table 2 quantifies this phenomenon. Without STATCOM, the overcurrent on feeder D3 exceeds the relay pickup threshold (1.5 × nominal) for approximately 60 ms (3 cycles at 50 Hz). Given that typical instantaneous overcurrent relays operate within 20 ms (1 cycle), depending on relay settings, this duration is sufficient to trigger an unwanted trip of feeder D3, potentially leading to cascading outages.

With STATCOM compensation, the overcurrent duration is reduced to less than 10 ms (0.5 cycles), which lies below the relay operating time. Therefore, the STATCOM effectively mitigates the multi-feeder protection coordination issue by:

(i) Rapidly restoring the voltage at the PCC.

(ii) Reducing the magnitude and duration of the transient overcurrent.

(iii) Allowing protection relays to remain selective (only the faulty feeder is disconnected).

Table 2 Protection relay response with and without STATCOM

Parameter	Without STATCOM	With STATCOM
Overcurrent duration (above 1.5 x I_{nom})	≈ 60 ms (3 cycles)	≈ 10 ms (0.5 cycle)
Typical relay operating time	20 ms (1 cycle)	20 ms (1 cycle)
Relay trip decision	Trip (unwanted)	No trip
Consequence	Cascading outage risk	Selective protection maintained

Thus, beyond standard oscillation damping, the STATCOM provides a specific protection coordination benefit unique to multi-feeder configurations: preventing nuisance tripping of healthy feeders. By rapidly restoring the voltage at the PCC, the STATCOM reduces the duration of transient overcurrents below the typical operating times of protection relays. This ensures that only the faulty feeder is disconnected, while the remaining feeders continue to operate normally. This selective protection is particularly important in networks with multiple outgoing feeders, where an unnecessary trip could lead to cascading outages and significant economic losses. The STATCOM therefore contributes not only to transient stability but also to the overall reliability of the protection system.

(3) Overvoltage severity and insulation coordination

The simulated overvoltage reaches 1.63 pu at the multi-feeder node. According to IEC 60071-1 [28], the switching impulse withstand voltage for equipment is generally above 2.0 pu. Therefore, the 1.63 pu peak remains below the withstand limit, and no catastrophic insulation failure occurs.

Regarding surge arresters, IEEE C62.11 [29] specifies that metal-oxide surge arresters for this voltage level typically clamp overvoltages at approximately 2.5 pu. The simulated peak of 1.63 pu is significantly lower than this clamping level. Therefore, even without STATCOM, the arrester would not trigger. Consequently, the observed protection coordination issues and power oscillations underscore the need for STATCOM.

This overvoltage results from a deliberately weak-grid worst-case scenario (low short-circuit level at the node). With STATCOM compensation, the voltage remains below 1.0 pu, substantially mitigating the issue. This confirms that the STATCOM is capable of effectively managing overvoltages even under severe network conditions, thereby enhancing the overall resilience of the system.

4. Conclusions

This study examined the transient response of an electrical network after losing a feeder at a multiple-feeder node. Using mathematical modeling with fifth-order and sixth-order differential equations and numerical simulation with the fourth-order Runge-Kutta method, the voltage behavior at the critical node was analyzed for the Liouesso-Ouesso network case study. The performance of STATCOM integration was assessed by comparing system responses with and without compensation. The following conclusions are drawn from this work:

(1) Equipment failure at a multi-feeder node causes large-amplitude power oscillations and transient overvoltages that greatly exceed normal levels (from 1.0 pu to nearly 1.63 pu), lasting for about three cycles (60 ms at 50 Hz). These disturbances may exceed the operating times of some fast-acting protection devices and increase the risk of cascading failures.

(2) Integrating the STATCOM at the critical node significantly shortens the oscillation duration (approximately 10 ms) and substantially attenuates residual oscillations. This results in a sixfold decrease in settling time compared to the uncompensated case.

(3) The transmitted power between nodes quickly returns to steady state with STATCOM compensation, preventing thermal and mechanical stress on transmission lines that occurs in the uncompensated case.

(4) STATCOM effectively protects sensitive equipment from network disturbances. For induction motors connected to nearby feeders, fluctuations in speed and electromagnetic torque are significantly reduced, maintaining mechanical integrity and improving operational continuity of industrial processes.

These results demonstrate that STATCOM is an effective solution for improving power system stability and resilience at multi-feeder nodes, while also enhancing protection coordination by preventing nuisance tripping of healthy feeders. A limitation of this study is the assumption of an ideal STATCOM, neglecting switching losses, harmonic generation, and PWM delays. Future work will incorporate a more detailed switching model, including harmonic analysis (IEEE 519 compliance), as well as integrate additional FACTS devices and advanced STATCOM control strategies (e.g., adaptive control or AI-based methods) to enhance power system robustness across various operating conditions.

Conflicts of Interest

The authors declare no conflict of interest.

References

[1] Y. Besanger, "Towards Improving the Security of Electric Power Networks," Ph.D. dissertation, National Polytechnic Institute of Grenoble, Grenoble, France, 2006.

[2] A. F. Snyder, "GPS-Synchronized Measurements for Damping Power Oscillations in Large Interconnected Electrical Networks," Ph.D. dissertation, National Polytechnic Institute of Grenoble, France, 1999.

[3] M. Gogom, A. O. Ganongo, N. Apila, and D. Lilonga-Boyenga, "Optimization of Power Transit through a Double-Term Line Term by the UPFC," Science Journal of Energy Engineering, vol. 8, no. 4, pp. 44-53, 2020.

[4] A. O. Ganongo, R. Gomba, Nianga-Apila, L. L. A. Obita, B. J. L. Makanga, M. Gogom, et al., "Influence of Electrode Spacing on Grounding Resistances in Electrical Networks for Effective Lightning Protection," Advances in Technology Innovation, vol. 11, no. 2, pp. 140-149, 2026.

[5] A. O. Ganongo, M. Gogom, Nianga-Apila, L. L. A. Obita, and G. Ganga, "Optimisation of Lightning Current Discharge to the Ground in Electrical Networks: Introduction of the Proportionality Coefficient (K)," Electric Power Systems Research, vol. 231, article no. 110348, 2024.

[6] V. Smith, V. Ilango, S. Perera, V. Gosbell, and D. Robinson, "Transient Overvoltages on the Electricity Supply Network - Classification, Causes and Propagation," Integral Energy Power Quality and Reliability Centre, University of Wollongong, Australia, 2005.

[7] J. Follum, F. Tuffner, L. Dosiek, J. Pierre, and E. S. Andersen, "Power System Oscillatory Behaviors: Sources, Characteristics, & Analyses," Pacific Northwest National Laboratory (PNNL), Technical Report PNNL-26644, 2017.

[8] D. Fulchiron, "Overvoltages and Insulation Coordination," Merlin Gerin, Technical Report 151, 1992.

[9] H. Nguyen Duc, "Improvement of Power Oscillation Damping in the Electrical Network with FACTS Devices and Remote Measurements," Ph.D. dissertation, School of Advanced Technology, University of Quebec, Canada, 2011.

[10] S. Ammari, "Interaction of FACTS Devices with Dynamic Loads in Transmission and Interconnection Networks," Ph.D. dissertation, Grenoble Institute of Technology, France, 2000.

[11] B. H. Alajrash, M. Salem, M. Swadi, T. Senjyu, M. Kamarol, and S. Motahhir, "A Comprehensive Review of FACTS Devices in Modern Power Systems: Addressing Power Quality, Optimal Placement, and Stability with Renewable Energy Penetration," Energy Reports, vol. 11, pp. 5350-5371, 2024.

[12] F. L. Probst, M. Beltle, M. Gerber, S. Tenbohlen, and K. A. Alsdorf, "Measurement of Switching Transient Overvoltages with a Capacitive Electric Field Sensor," Electric Power Systems Research, vol. 223, article no. 109619, 2023.

[13] E. A. R. L. Pannila and M. Edirisinghe, "Signatures of Transient Overvoltages in Low Voltage Power Systems in Tea Factories and Their Implications on Insulation Deterioration and Allied Power Quality Issues," Journal of Electrical and Computer Engineering, vol. 2021, article no. 2623965, 2021.

[14] F. H. B. Bittar, A. P. L. Barbero, V. H. Ferreira, A. B. dos Santos, D. S. de Souza, A. da Costa Pinho, et al., "Neglected Frequencies Analysis on Switching Operations in Extra-High Voltage Electrical Power Substations," Electric Power Systems Research, vol. 225, article no. 109848, 2023.

[15] S. K. E. Awadallah, S. Mohanty, and F. Ghassemi, "Transient Overvoltage Transfer and Amplification in a 400kV Network – A Case Study," Electric Power Systems Research, vol. 223, article no. 109583, 2023.

[16] C. Zhang, S. Xie, Q. Chen, Z. Mu, Y. Xia, L. Zhou, et al., "Feature Statistics and Analysis of Transient Overvoltage Waveform Measured From 220 kV Substation," International Journal of Electrical Power & Energy Systems, vol. 158, article no. 109824, 2024.

[17] R. Devarapalli and B. Bhattacharyya, "Power and Energy System Oscillation Damping Using Multi-Verse Optimization," SN Applied Sciences, vol. 3, article no. 383, 2021.

[18] J. Bhukya and V. Mahajan, "Optimization of Controllers Parameters for Damping Local Area Oscillation to Enhance the Stability of an Interconnected System with Wind Farm," International Journal of Electrical Power & Energy Systems, vol. 119, article no. 105877, 2020.

[19] G. Zhang, W. Hu, D. Cao, J. Yi, Q. Huang, Z. Liu, et al., "A Data-Driven Approach for Designing STATCOM Additional Damping Controller for Wind Farms," International Journal of Electrical Power & Energy Systems, vol. 117, article no. 105620, 2020.

[20] W. Peres and N. N. da Costa, "Comparing Strategies to Damp Electromechanical Oscillations through STATCOM with Multi-Band Controller," ISA Transactions, vol. 107, pp. 256-269, 2020.

[21] S. Bamba and G. S. Kumar, "Enhancing Power System Stability through Intelligent STATCOM Control Strategies in Torsional Oscillation Environments," Sigma Journal of Engineering and Natural Sciences, vol. 42, no. 6, pp. 1933-1953, 2024.

[22] K. Kouider and A. Bekri, "Enhancing Transient Stability and Dynamic Response of Wind-Penetrated Power Systems through PSS and STATCOM Cooperation," International Journal of Renewable Energy Development, vol. 12, no. 5, pp. 816-831, 2023.

[23] X. Jiang, H. Yi, Y. Li, F. Zhuo, Z. Wang, D. Yu, et al., "Low-Frequency Oscillation Damping of Grid-Forming STATCOMs with Phase-Compensated DC-Link Voltage Synchronization," IEEE Transactions on Power Electronics, vol. 40, no. 2, pp. 2860-2873, 2025.

[24] K. Hasan, M. M. Othman, S. T. Meraj, Md. S. Rahman, M.S. H. Lipu and M. R. Sarker, "Emerging Power Quality Improvement Technology: Recent Advances on Topologies, Control Schemes, Issues and Prospects Towards Grid Decarbonization", Results in Engineering, vol. 29, article no. 109256, 2026.

[25] P. Petitclair, "Modeling and Control of FACTS (Flexible Alternative Current Transmission System) Structures: Application to STATCOM (STATic COMPensator)," Ph.D. dissertation, National Polytechnic Institute of Grenoble, France, 1997.

[26] O. Reffas, "Improving the Efficiency of a Reactive Power Compensation Installation," Ph.D. dissertation, Badji Mokhtar University Annaba, Algeria, 2020.

[27] Y. Merzoug, "Optimal Control of Reactive Powers and Voltages in an Electrical Energy Network by FACTS Devices," Ph.D. dissertation, University of Science and Technology of Oran Mohamed Boudiaf, Algeria, 2014.

[28] IEC 60071-1:2019, "Insulation Co-ordination – Part 1: Definitions, Principles and Rules," International Electrotechnical Commission, Geneva, 2019.

[29] IEEE C62.11-2020, "IEEE Standard for Metal-Oxide Surge Arresters for AC Power Circuits (>1 kV)," IEEE Power and Energy Society, New York, 2020.

Appendix

A.1 Calculation of parameters for the equivalent diagram presented in Fig. 8

(1) Thevenin source and equivalent impedance

The upstream network, consisting of the source and equivalent impedance seen from busbar JB1, is reduced to a Thevenin equivalent circuit. This simplification allows the entire upstream system to be represented as a single voltage source.

$$v_{Th}(t) = V_{Th}\sin(\omega t + \theta),\ \ V_{Th} = \frac{\sqrt{R_{D1}^2 + X_{D1}^2}}{\sqrt{R_{D1}^2 + (X_{D1} + X'_d)^2}} V_s$$

$$\theta = \arctan\frac{X_{D1}}{R_{D1}} - \arctan\frac{X_{D1} + X'_d}{R_{D1}}, \qquad Z_{Th} = (j\omega L'_d) \parallel Z_{D1} = R_{Th} + j\omega L_{Th}$$

(2) Transformer turns ratios

$$a_{T1} = \frac{U_{JB1}}{U_{JB2}}, \quad a_{T2} = \frac{U_{JB3}}{U_{JB4}}$$

(3) Parameters of transformer 1-2 referred to the secondary side of transformer T2

For this transformer, the parameters are first referred to its own secondary side (110 kV) and are subsequently referred to the secondary side of transformer T2 (30 kV) by means of the turns ratio of T2.

$$Z_{T12} = \frac{U_{cc}\%}{100} \cdot \frac{U_{JB2}^2}{S_{T12}}, \quad R_{T12} = \frac{P_{cu}}{I_{n2}^2} = \frac{P_{cu} \cdot U_{JB2}^2}{S_{T12}^2}, \quad X_{T12} = \sqrt{Z_{T12}^2 - R_{T12}^2}$$

$$R_{12} = \frac{R_{T12}}{2 \cdot a_{T2}^2}, \quad X_{12} = \frac{X_{T12}}{2 \cdot a_{T2}^2}, \quad L_{12} = \frac{X_{T12}}{2\pi f}$$

(4) Parameters of transformers 3-4 referred to the secondary side of transformer T2

For transformer T2, since its secondary side is at 30 kV, its parameters are referred directly to its secondary side.

$$Z_{T34} = \frac{U_{cc}\%}{100} \cdot \frac{U_{JB4}^2}{S_{T34}}, \quad R_{T34} = \frac{P_{cu}}{I_{n1}^2} = \frac{P_{cu} \cdot U_{JB4}^2}{S_{T34}^2}, \quad X_{T34} = \sqrt{Z_{T34}^2 - R_{T34}^2}$$

$$R_{34} = \frac{R_{T34}}{2}, \quad X_{34} = \frac{X_{T34}}{2}, \quad L_{34} = \frac{X_{34}}{2\pi f}$$

(5) Thevenin source and equivalent impedance referred to the secondary side of transformer T2

The Thevenin equivalent is expressed on the primary side of transformer T1. To refer it to the secondary side of T2 (30 kV), both transformation ratios (that of T1 and that of T2) have been applied.

$$v'_{Th}(t) = \frac{v_{Th}(t)}{a_{T1} \cdot a_{T2}}, \quad Z'_{Th} = \frac{Z_{Th}}{a_{T1}^2 \cdot a_{T2}^2} = R'_{Th} + j\omega L'_{Th}$$

(6) Line parameters (resistance, inductance, and capacitance) referred to the secondary side of transformer T2

The line resistance, inductance, and capacitance have been referred to the secondary side of transformer T2 (30 kV) using the square of the turns ratio.

$$R'_{23} = \frac{R_{23}}{a_{T2}^2}, \quad X'_{23} = \frac{X_{23}}{a_{T2}^2}, \quad C'_{12} = \frac{C_{23}}{a_{T2}^2}$$

(7) Line parameters combined with those of the transformers

The line parameters (resistance, inductance, and capacitance) are first referred to the secondary side of transformer T2 (30 kV). The equivalent resistance and inductance are then obtained by adding the referred line parameters to the referred transformer parameters (which have already been referred to the secondary side of T2). The total equivalent capacitance is that of the line alone, since the transformers do not contribute to the capacitance.

$$R = R_{12} + R'_{23} + R_{34}, \quad L = L_{12} + L'_{23} + L_{34}$$

A.2 Induction motor parameters

Table A.1 lists the numerical parameters of the induction motor connected to feeder 3, as used in the MATLAB simulation (Section 3.1, Figs. 11-12).

Table A.1 Induction motor parameters used in MATLAB simulation

Parameter	Value	Unit	Parameter	Value	Unit
Stator resistance	0.15	Ω	Stator current	30.16	A
Rotor resistance	0.30	Ω	Rotor current	24.68	A
Stator inductance	0.045	H	Useful torque	46.46	N·m
Rotor inductance	0.045	H	Rotor Joule losses	548.17	W
Mutual inductance	0.0425	H	Stator Joule losses	409.27	W
Moment of inertia	0.15	$kg \cdot m^2$	Input power	15.29	kW
Rated voltage	381	V	Output power	14.06	kW
Frequency	50	Hz	Efficiency	91.9	%